Published in : Journal of Materials Science: Materials in Electronics (2025), vol. 36, n°28, 1836
DOI: 10.1007/s10854-025-15900-x
Status : Postprint (Author's version)

EFFECTS OF CARBON NANOTUBES ON THE AC CONDUCTIVITY, PERMITTIVITY, AND ELECTROMAGNETIC SHIELDING PERFORMANCE OF POLYURETHANE FOAMS IN THE 15 HZ–26.5 GHZ FREQUENCY RANGE

Ahmad Mamoun Khamis[1] , Laetitia Urbanczyk[2], Christophe Detrembleur[2,3], and Isabelle Huynen[1]

[1]*ICTEAM Institute, Université Catholique de Louvain, 1348 Louvain-La-Neuve, Belgium*
[2]*Center for Education and Research On Macromolecules (CERM), CESAM Research Unit, University of Liege, Sart-Tilman B6a, 4000 Liege, Belgium*
[3]*WEL-T Research Institute, Avenue Pasteur, 6, 1300 Wavre, Belgium*

ABSTRACT

This study investigates the impact of increasing carbon nanotube (CNT) concentration on the AC conductivity, dielectric, and electromagnetic shielding properties of polyurethane (PU) foams. Four CNT-PU foam samples with different CNT contents (1 wt.%, 2.3 wt.%, 6 wt.%, and 11.2 wt.%) were fabricated using the dip coating method. Three different measurement techniques were employed to characterize the AC conductivity and complex permittivity of the CNT-PU composites across various frequency ranges (kHz, MHz, and GHz). COMSOL software was also used to calculate the scattering parameters and visualize the electric field distribution. The microstructure SEM images of CNT-PU samples confirmed that the CNTs formed interconnected and well-distributed networks on the PU surface skeleton, leading to conductive pathways that boost the absorption loss. Therefore, increasing CNT content increased the permittivity and conductivity of CNT-PU samples, and consequently, the total shielding effectiveness (SE_T). The incorporation of 11.2 wt.% CNT greatly enhanced the AC conductivity, increasing it from 3.6×10^{-6} S/cm (pure PU) to 0.0068 S/cm at 10 MHz. Furthermore, the corresponding values of complex permittivity also increased from 1.32—j 0.0059 to 8.65—j 3.7 at 1000 MHz. The complex permittivity of 11.2 wt.% CNT sample was 3.76—j 3.56 at 25 GHz. The samples with 6 wt.% CNT and 11.2 wt.% CNT met the standard requirements for the electromagnetic interference shielding applications because their total shielding effectiveness (SE_T) values surpassed the 20 dB threshold within the 18–26.5 GHz frequency range. The visualization of the electric field distribution further confirmed that the 11.2 wt.% CNT sample greatly attenuated the electric field propagation through the material. The contribution of the absorption loss mechanism to the SE_T of CNT-PU samples surpassed 94% in the 18–26.5 GHz frequency range, indicating that the absorption loss was the main shielding mechanism in our samples.

Published in : Journal of Materials Science: Materials in Electronics (2025), vol. 36, n°28, 1836
DOI: 10.1007/s10854-025-15900-x
Status : Postprint (Author's version)

1. Introduction

Electromagnetic interference (EMI) is a critical problem for communication systems and modern electronic devices, often causing reduced performance, data corruption, and malfunction [1]. EMI is created by external electromagnetic (EM) waves that interrupt the standard operation of electronic devices. Therefore, it is crucial to develop EMI shielding materials that can operate over a wide range of sectors such as aerospace, medical, electronics, defence, and automotive [2]. Metals are conventionally used for EMI shielding because of their high conductivity. Nevertheless, they are heavy, hard to process, and vulnerable to corrosion [3]. Therefore, polymer composites have emerged as an alternative solution to the metal-based EMI shielding. The advantage of polymer-based composites, compared to metal materials, is the manufacturing process that enables the production of complex shapes with lower density, leading to lower fuel consumption (for automobile and aviation) and higher speed in competitive sport [4]. Additionally, polymer composites showed outstanding EMI shielding performance for construction, aerospace, electronics, and medical market [5]. It is challenging to design conductive polymer composites (CPCs) because over-shielding leads to higher sample cost, while under-shielding could cause a product failure. There are three mechanisms involved in EMI shielding: absorption, reflection, and multiple reflections. Absorption depends on the shield's thickness, and it increases with increasing concentration of magnetic or electrical dipoles that can dissipate the EM energy. The reflection is the primary shielding mechanism in a homogeneous conductive material, and the multiple reflection is the internal reflection within the shielding sample [6]. Conductive fillers such as carbon black, carbon nanotube (CNT) [7], graphite, and graphene [8] are added to polymers to form the conductive polymer composites.

In the twenty-first century, nanotechnology is considered one of the most promising techniques. This technology involves transforming the nanoscience theories into practical applications by controlling, assembling, manipulating, and manufacturing samples at the nanoscale [9]. Nanostructure refers to structures or materials which have at least one dimension between 1 and 100 nm. These structures are fabricated using simple and complicated methods [10]. The very rapid development of nanoscience confirms that the manufacturing at the nanoscale will be integrated into all fields of technology and science. With development in science and technology, researchers embrace products and technologies which are cheaper, cleaner, and safer than previous technologies [11]. Currently, nanotechnology is widely used in several industries and fields such as electronics, medicine, printing, textiles, agriculture, automotive, construction, and renewable energy [12]. A wide variety of nanomaterials have recently been developed for various applications such as sensing, catalysis, optoelectronics, and electronics [13]. In this study, carbon nanotubes were used to prepare the samples because their fibrous structures with high-aspect ratios are suitable as EMI shielding materials [14]. In addition, the polymer foams are widely used in many applications such as protective equipment, furniture cushioning, packaging of food, thermal insulation of medical devices, and transportation [15]. The CNT fillers can be incorporated into different polymers for EMI shielding applications, such as polypropylene (PP) [6], isotactic PP, high-density polyethylene (HDPE) [16], PU foam [17], polycarbonate (PC) [18], polycaprolactone (PCL)

Published in : Journal of Materials Science: Materials in Electronics (2025), vol. 36, n°28, 1836
DOI: 10.1007/s10854-025-15900-x
Status : Postprint (Author's version)

[19], and polylactic acid (PLA) [20]. However, PU foam is used in this study because it has unique properties such as low weight, low cost, and porosity, that influences the multireflection of EM waves inside the material [21]. The conductive PU composites can also be found in other applications, such as environmental and medical sensing, electrochemical energy storage, and tissue regeneration [22]. Additionally, the CNT-PU nanocomposites have been studied in various fields such as bone substitution, cardiovascular applications, ligament, tendon, and neural tissue engineering [23]. The CNT-foam samples can be fabricated using two main methods. In the first one, which is called the bottomup method, the CNTs are directly dispersed into the polymer matrix, followed by the foaming process. In the second method, the CNTs are deposited (dip coating) onto a ready-made foam sample [24]. In this research, the latter method was used to fabricate the CNT-PU foam samples.

The electromagnetic properties of CNT-PU foams, fabricated via the bottom-up method, were studied in different frequency ranges such as 10^2–10^6 Hz [25], 30 MHz–1.5 GHz [26], and 2–18 GHz [27]. On the other hand, studies on CNT-PU samples, prepared using the second method, focused on the engineering scaffolds [28], wearable pressure sensors [29], and damping applications [30]. It is important to note that the number of EM applications (such as EMI shielding) in which a certain material can be used depends on its EM properties at specific frequency ranges. Therefore, investigating the EM properties over a broad frequency range will increase the number of applications where the material may be used, compared to a narrow frequency range. This study investigates the interaction between the EM waves and CNT-PU samples, prepared using the second method, in three different frequency ranges (kHz, MHz, and GHz). Several applications are covered in these frequency ranges, including marine communications in the 30–300 kHz range, television, microwave, and mobile phones in the 300 MHz–1 GHz range, and satellite communications in the 10–26.5 GHz range [5]. Therefore, three different setups were used to characterize the samples. Such characterizations are crucial for enabling CNTPU samples to be used in a wide range of frequencies. To the best of our knowledge, foamed samples have never been characterized using the Dielectric Material Test Fixture (DMTF) because the upper electrode always presses the material under test (MUT). Such pressing decreases the thickness of the foam sample under test, leading to the following problems: the content of air inside the foam sample will decrease, which may result in wrong values of dielectric constant; it is not possible to measure the new thickness of the foam sample after the upper electrode presses the foam sample, and finally it is not possible to obtain the real dielectric constant of the MUT since a significant change in dimensions occurred. Thus, we developed a 3D holder to maintain a constant distance of 2.5 mm between the upper and lower electrodes, which will overcome the limitations of characterizing foam samples using DMTF. Therefore, this study presents, for the first time, the characterizations of foam samples using DMTF.

This research aims to fabricate and characterize CNT-PU samples for EMI shielding applications. These applications are applied in several industries such as microelectronics, computer, automotive, and aerospace [5]. The novelty of this work lies in the following aspects : 1- The usage of DMTF to characterize foam samples. 2- Investigating the electromagnetic properties of CNT-PU foam samples over a broad frequency range from 15 Hz to 26.5 GHz. 3- Visualizing the effects of increasing CNT concentrations on the electric field distribution of CNT-PU samples. The AC conductivity of CNT-PU samples is studied in the 15 Hz to 10 MHz frequency range. The permittivity

Published in : Journal of Materials Science: Materials in Electronics (2025), vol. 36, n°28, 1836
DOI: 10.1007/s10854-025-15900-x
Status : Postprint (Author's version)

results are also presented in the 10 MHz–1 GHz and 10–25 GHz frequency ranges. In addition, COMSOL Multiphysics was used to calculate the scattering parameters (S_{11} and S_{21}) and visualize the electric field distribution (EFD) of CNT-PU samples in the 18–26.5 GHz frequency range. The impact of CNT concentrations on the EFD inside CNT-PU samples has not been studied previously using COMSOL. Five simulations were conducted to investigate the effects of CNTs content on the intensity and distribution of the electric field.

2. Materials and methods

2.1. MATERIALS

Two materials were used in the fabrication of the CNT-PU foam samples:

1. AQUACYL™ AQ0303 waterborne dispersions of multiwall carbon nanotubes (Nanocyl SA, Sambreville, Belgium).
2. Open-cell polyurethane foam with a net density of 54 kg/m^3 (SiPLA SA, Wavre, Belgium). The average pore diameter is around 0.46 mm.

2.2. FABRICATION OF CNT-PU SAMPLES

In this study, the dip coating method is chosen for the fabrication of CNT-PU foam samples because of three advantages: it is the most cost-effective, the fabricated foam can be used directly without post-processing, and finally the foam is fully covered with the applied nanofiller. The dip coating method has been used in previous studies to coat foam samples with different fillers [31, 32]. The commercial CNT/water masterbatch Aquacyl 0303 was diluted with distilled water at specific ratios to prepare four different CNT solutions. The dilution factors used were 1/40, 1/20, 1/10, and 1/4 for a total volume of 1200 ml. Then, the pure PU foam was immersed in the diluted CNT solution for twenty-four hours. A weight of 1 kg was applied to the foam's surface to immerse the sample, and it was squeezed 5 times during the first hour to enhance the penetration of liquid inside the foam. Afterwards, the sample was removed and dried in a vacuum oven for twenty-four hours at 70 °C. The weight difference between before and after the dipping process was used to deduce the amount of CNT incorporated into the PU foam. This procedure led to CNT-PU foam samples containing different CNT concentrations (1 wt.%, 2.3 wt.%, 6 wt.%, and 11.2 wt.%). The surface dimensions of each sample were (16 cm × 16 cm) with a thickness of 2 cm. Samples were prepared in a rigorous manner. The CNT concentration is estimated with 5% error due to the balance precision of 0.01 g used.

Published in : Journal of Materials Science: Materials in Electronics (2025), vol. 36, n°28, 1836
DOI: 10.1007/s10854-025-15900-x
Status : Postprint (Author's version)

3. Characterization and simulation methods

All measurements were performed at room temperature (22.5 °C). The scanning electron microscope (SEM) was used to examine the morphology of CNTPU samples. Novocontrol was used to characterize the AC conductivity. The impedance analyser and vector network analyser were used to characterize the permittivity.

COMSOL Multiphysics software was used to obtain scattering parameters and electric field distributions. Characterizing of CNT-PU samples, over a broad frequency range using multiple measurement techniques is a key novelty of this study.

3.1. MORPHOLOGY, ACCONDUCTIVITY, AND PERMITTIVITY MEASUREMENTS

The dispersion of CNTs on the surface of PU was investigated using JEOL 7600 F SEM (operating at 15 keV). The CNT-PU samples were coated with a gold layer using the Cressington sputter 208HR.

The AC conductivity of CNT-PU samples was measured in the 15 Hz to 10 MHz frequency range using Alpha-A Analyzer (Novocontrol) connected to a Dielectric Test Fixture (Agilent, 16451B). This system uses the parallel plate method that sandwiches the MUT between two electrodes to form a capacitor [33] as shown in Fig. 1. The measurements were conducted using Novocontrol Windows-based WinDETA software, which supports dielectric, impedance, conductivity, and gain phase measurements. The accuracy of the results was validated by measuring a reference material (PTFE) before conducting the measurement on the CNT-PU samples. The thickness of each sample was 4 mm. The uncertainty in the sample geometry was provided by the manufacturer as follows: for a sample with a thickness of 0.1 mm, the error in the thickness has to be less than 1 µm for a 1% accurate result.

The Dielectric Material Test Fixture (Keysight, 16453 A) connected to the Impedance Analyzer (Keysight, E4991B) was used to measure the relative permittivity (ε'—jε") of CNT-PU samples in the 10 MHz–1 GHz frequency range at room temperature (22.5 °C). The measurement setup is presented in Fig. 2. This test fixture employs the parallel plate capacitor method [34]. Calibration was performed in three stages: open, short, and load. In the first stage (open), the knob was pulled up and the latch button was pressed while holding up the knob. The second stage was performed after releasing the latch button, so the upper electrode contacted the lower one. A PTFE sample with 0.770 mm thickness was used as a load to perform the third stage of calibration. It was also used as a reference material to confirm the calibration accuracy. Initially, it was not possible to measure the foamed CNT-PU samples using the standard DMTF because the upper electrode always compresses the MUT, which cannot keep its initial thickness and air content. Hence, we designed a novel 3D holder to keep the knob holding up. With the 3D holder in place, the distance between the electrodes matched the samples' thickness of 2.5 mm.

Measurement accuracy of the impedance analyzer applies when the calibration is performed at 23 °C ± 5 °C. When the calibration is below 18 °C or above 28 °C, the measurement error doubles. The

Published in : Journal of Materials Science: Materials in Electronics (2025), vol. 36, n°28, 1836
DOI: 10.1007/s10854-025-15900-x
Status : Postprint (Author's version)

basic accuracy is ± 0.65% and the impedance range is 120 mΩ to 52 kΩ (10% measurement accuracy range).

Fig. 1. *Dielectric Test Fixture setup for AC conductivity measurements in the 15 Hz to 10 MHz frequency range*

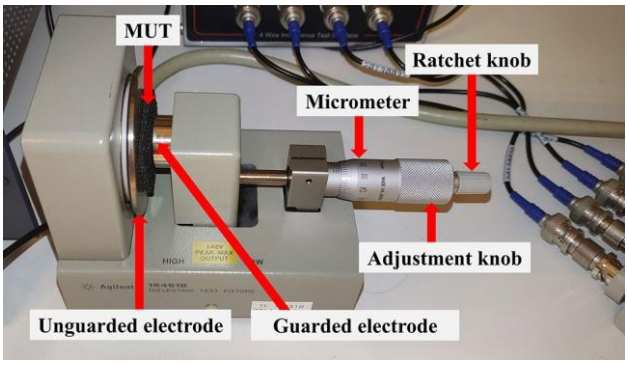

Fig. 2. *Keysight impedance analyser connected to the DMTF for permittivity measurements in the 10 MHz–1 GHz frequency range*

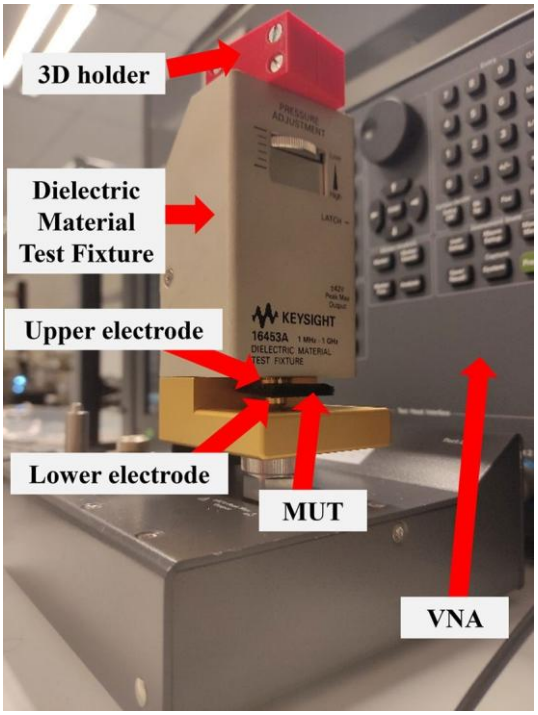

The relative permittivity (ε'—j ε") of CNT-PU samples was measured using the vector network analyzer (VNA, Keysight, N5242B) connected to an OECP (Performance probe kit) in the 10–25 GHz frequency range. The typical power level accuracy (dB) of the VNA is ± 0.60 for the 10–18 GHz frequency range. The Agilent (N4691) Electronic Calibration (ECal) was connected in line between the OECP and the VNA, as shown in Fig. 3. The "Coaxial Probe Method" option was selected in the Keysight Materials Measurement Suite. The calibration stages were as follows: Open, short, and distilled water, for 201 points, at room temperature (22.5 °C). After performing the calibration, two different reference materials (water and isopropanol) were used to validate the calibration accuracy.

Published in : Journal of Materials Science: Materials in Electronics (2025), vol. 36, n°28, 1836
DOI: 10.1007/s10854-025-15900-x
Status : Postprint (Author's version)

The measurements of CNT-PU samples were conducted with free-gap contact between the MUT and the probe.

Fig. 3. *Keysight N5242B VNA connected to an OECP for permittivity measurements in the 10–25 GHz frequency range*

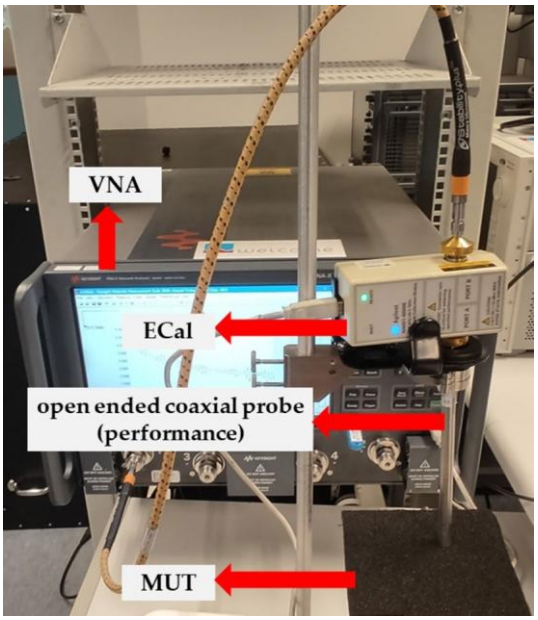

3.2. COMSOL SIMULATIONS

COMSOL Multiphysics 6.2 is a Finite Element Method (FEM) software. The FEM divides the continuous spatial domain under scope into a finite number of small modules, set up each module of the formula and solve it, then combine them [35]. In our study, the permittivity values of CNT-PU samples measured using the VNA connected to the OECP were used to calculate the scattering parameters (S_{11} and S_{21}) and visualize the electric field distribution using COMSOL. The simulated WR42 waveguide has the dimensions of 1.0668 cm × 0.4318 cm [36], and it covers the 18–26.5 GHz frequency range. The waveguide geometry was divided into three sections as shown in Fig. 4, where a sample thickness of 1 cm is considered.

The process for building and simulating the CNTPU geometry was conducted using the following steps. The Model Wizard with 3D model was selected. Then, the Radio Frequency module with Electromagnetic Waves and Frequency Domain was assigned. Next step, the geometry was built using the Geometry interface, and the EM properties were stated in Materials. The boundary conditions were then introduced as Perfect Electric Conductor, and the two ports were defined. The meshing was generated with Finer element size for higher accuracy, before configuring the frequency range and executing the study (Compute). Finally, the results were exported in terms of scattering parameters and electric field distribution.

Published in : Journal of Materials Science: Materials in Electronics (2025), vol. 36, n°28, 1836
DOI: 10.1007/s10854-025-15900-x
Status : Postprint (Author's version)

Fig. 4. *The waveguide regions in COMSOL simulation*

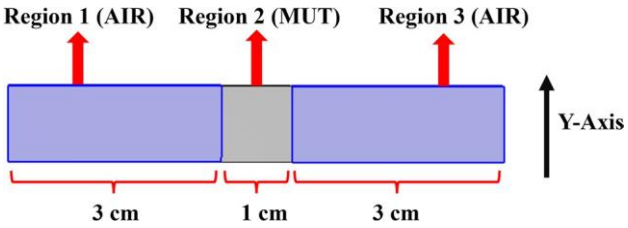

4. Results and discussion

This section presents the surface morphology examined using SEM, AC conductivity measured using Novocontrol system connected to a Dielectric Test Fixture in the 15 Hz–10 MHz frequency range, complex permittivity characterized using an impedance analyzer connected to a DMTF and VNA system connected an OECP in the frequency ranges of 10–1000 MHz and 10–25 GHz, respectively. The scattering parameters obtained using COMSOL Multiphysics are also presented, together with the related SE_T calculations and EFD visualization.

4.1. SURFACE MORPHOLOGY OF CNT-PU SAMPLES

The SEM was used to examine the morphology of CNT-PU composites. The SEM images, shown in Fig. 5, shared the same magnification scale of 50k. The PU matrix exhibits a smooth skeleton as also reported in the previous study [37]. The gold coating, described in Section 3.1, caused the cracks visible in Fig. 5a. The CNTs are clearly visible and evenly distributed on the samples' surfaces with no accumulation, as shown in the images of Fig. 5(b, c, d, and e). These images also do not show the PU surfaces, proving that the CNT network covered all PU surfaces in the CNT-PU samples without interruption. The images of CNTPU samples also confirm that the CNT fillers are not isolated. Furthermore, the CNTs were intertwined with each other to establish interconnected networks as presented in the images of Fig. 5(b, c, d, and e). The conductive path of CNT-polymer composites is established by CNTs that are in contact with each other [38]. The SEM images of our CNT-PU samples confirm that the CNTs are in contact together, leading to a conductive path on the surface. The interconnected networks were successfully formed in the 1 wt.% CNT specimen that had the lowest concentration of CNT. Therefore, we cannot see a noticeable change in morphology with increasing CNT content because the SEM only examines the sample's surface. Hence, increasing the CNT content leads to denser conductive networks of CNT. Consequently, the greatest rise in conductivity, complex permittivity, and SE_T, presented in the subsections below, was recorded between the two samples of PU and 1 wt.% CNT. This is because the percolated networks of CNT were already built at 1 wt.% CNT sample, leading to an uninterrupted conductive pathway.

Published in : Journal of Materials Science: Materials in Electronics (2025), vol. 36, n°28, 1836
DOI: 10.1007/s10854-025-15900-x
Status : Postprint (Author's version)

4.2. AC CONDUCTIVITY IN THE 15HZ—10MHZ FREQUENCY RANGE

The AC conductivity (σ_{ac}) of CNT-PU samples measured using the Novocontrol Analyzer in the 15 Hz–10 MHz frequency range is shown in Fig. 6. In this frequency range, the ohmic conduction dominates the electrical response below 100 kHz [39]. Increasing CNT contents significantly enhanced the σ_{ac}. At 10 MHz, the AC conductivity values of neat PU (no fillers) and 11.2 wt.% CNT samples were 3.6 × 10^{-6} S/cm and 0.0068 S/cm, respectively, which means that the σ_{ac} increased by more than 1800 times. These results are consistent with a study conducted by Hoang [40]. Ilya also reported that the AC conductivity of PU is approximately 10^{-6} S/cm within the 10^5–10^6 frequency range [41].Our CNT-PU samples are less conductive than copper since they did not reach the value of 1000 S/cm; however, they are not insulators because their AC conductivity is higher than 10^{-8} S/cm [42].

At 10 MHz, the σ_{ac} values were 0.00048 S/cm, 0.0012 S/cm, 0.0037 S/cm, and 0.0068 S/cm for the 1 wt.% CNT, 2.3 wt.%, 6 wt.%, and 11.2 wt.% samples, respectively. This indicates that the σ_{ac} increased by 150%, 208%, and 83% by increasing the CNT concentration from 1 wt.% to 2.3%, 2.3 wt.% to 6 wt.%, and 6 wt.% to 11.2 wt.%, respectively.

The AC conductivity is directly related to the frequency (f) and the imaginary part of permittivity (ε'') via the following equation [43]:

$$\sigma_{ac} = 2\pi\varepsilon_0 f\varepsilon'' \quad (1)$$

Where ε0 represents the free space permittivity. Based on Eq. 1, the σ ac is directly proportional to f and ε". Increasing CNT content in the samples thickened the CNT coatings on the surfaces, leading to additional conductive pathways which resulted in higher energy loss, ε", and AC conductivity. The additional conductive pathways also impacted on the increment behaviour of AC conductivity with frequency, where a sharper rise in AC conductivity occurs in samples with higher CNT content.

Published in : Journal of Materials Science: Materials in Electronics (2025), vol. 36, n°28, 1836
DOI: 10.1007/s10854-025-15900-x
Status : Postprint (Author's version)

Fig. 5. *SEM images of CNTPU samples, obtained using JEOL 7600 F SEM (operating at 15 keV); a: PU, b: 1 wt.% CNT, c: 2.3 wt.% CNT, d: 6 wt.% CNT, e: 11.2 wt.% CNT*

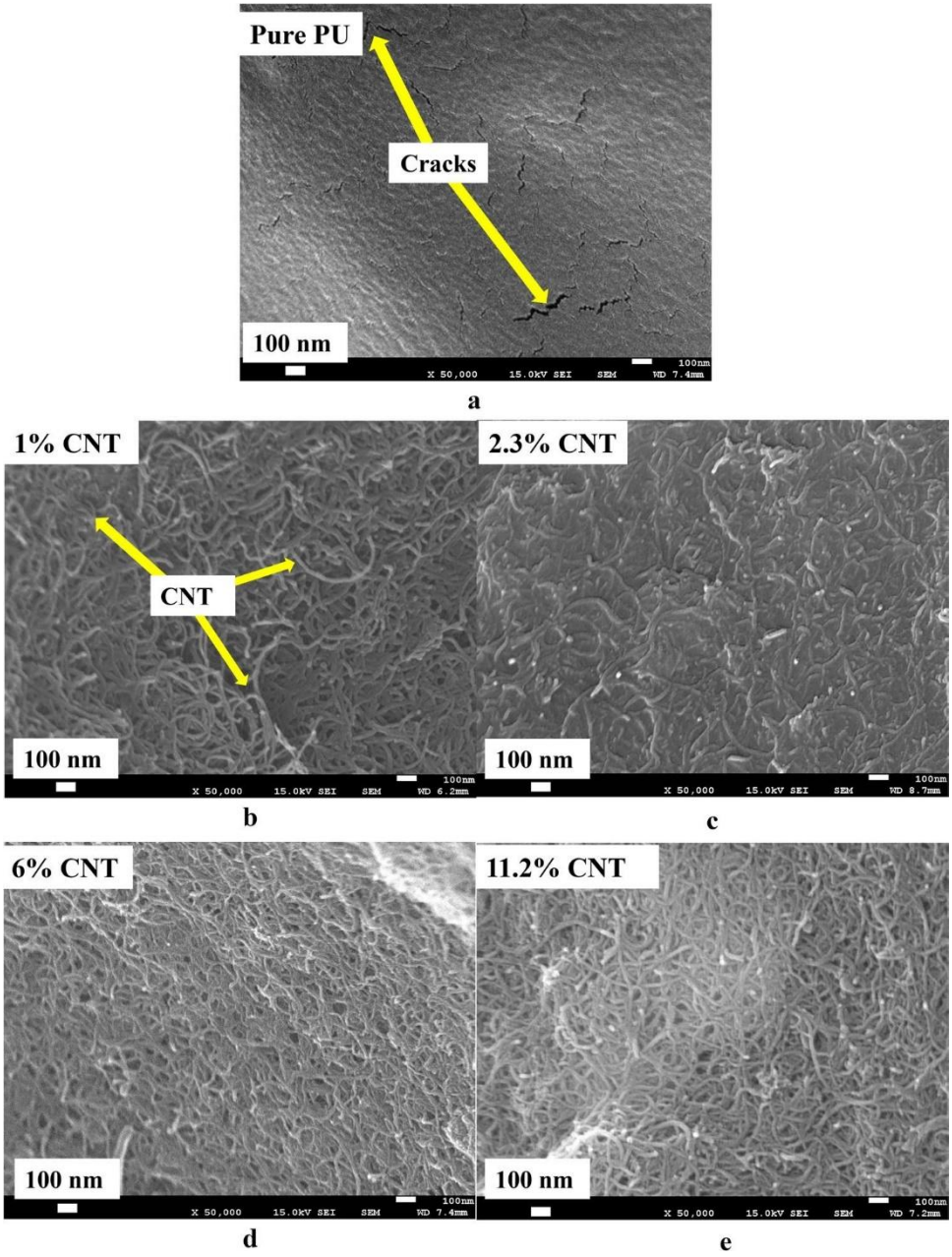

4.3. DIELECTRIC PROPERTIES IN THE 10–1000 MHZ FREQUENCY RANGE

The real part of permittivity (dielectric constant, ε') indicates the amount of energy stored by a certain material in a specific electric field relative to empty space, while the imaginary part of permittivity (loss factor, ε") shows how much of this energy can be converted into heat [44]. The ε' and ε'' are key indicators for analysing the wave absorption performance of composite materials [45]. The presence of the conductive CNT fillers in the electrically insulating matrix of PU significantly

Published in : Journal of Materials Science: Materials in Electronics (2025), vol. 36, n°28, 1836
DOI: 10.1007/s10854-025-15900-x
Status : Postprint (Author's version)

increases the permittivity (ε' and ε") of CNT-PU samples, as shown in Fig. 7 and Table 1. The ε' values of PU sample reported in this study are in accordance with the ones reported by Wang [46].

Fig. 6. *AC conductivity of CNT-PU samples measured using Alpha-A Analyzer (Novocontrol) connected to Dielectric Test Fixture, employing the parallel plate method, in the 15 Hz–10 MHz frequency range*

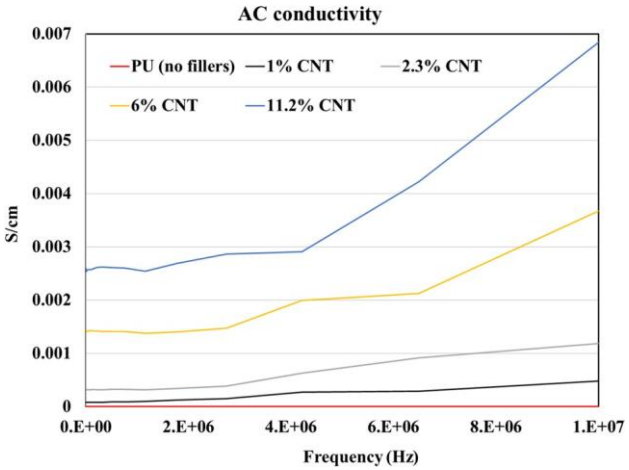

There are four polarization mechanisms known in dielectric materials such as PU matrix: interfacial, dipole-oriented, ionic, and electronic. However, each mechanism corresponds to a certain frequency range. For example, the interfacial polarization takes place in the low-frequency range while the electronic polarization occurs in the optical frequency range around 10^{15} Hz. Therefore, electronic polarization can be ignored in our study, but the effects of interfacial polarization could occur at the beginning of the MHz frequency range. In our samples, PU is a dielectric material while CNT is a conductive filler; therefore, the space charges accumulate at the interface between the CNT and PU contribute to the interfacial polarization (Maxwell–Wagner–Sillar) [47]. It is worth noting that the interfacial polarization in our samples may occur at the interface between PU and CNTs because a surface layer of CNTs was formed on the PU surface as confirmed in Sect. 4.1. The high permittivity at lower frequencies could be due to free charge built up at the interface between PU and CNT. Therefore, the permittivity decreased with increasing frequency because the periodic reversal of the electric field occurred so fast that there was no excess charge in the direction of the field, leading to a decrease in the interfacial polarization due to the charge accumulation decrement [48]. The PU has covalent bonds; therefore, the ionic polarization can also be excluded in this study. Dipole polarization could be dominant in our study because the urethane [–NH–CO–O–] group, which is the main building block of PU, exhibits a dipole moment. However, the permittivity of PU, shown in Fig. 7, is constant over the whole frequency range, which suggests that the dipolar relaxation took place below the measured frequency range. Moreover, the dielectric constant of PU, 1 wt.% CNT, and 2.3 wt.% CNT samples, shown in Fig. 7, is nearly frequency independent compared to 6 wt.% CNT and 11.2 wt.% CNT samples which are strongly dependent on frequency below 0.5 GHz. This is explained by the high concentration of CNT, which causes a denser conductive network, leading to stronger interfacial polarization.

Published in : Journal of Materials Science: Materials in Electronics (2025), vol. 36, n°28, 1836
DOI: 10.1007/s10854-025-15900-x
Status : Postprint (Author's version)

Fig. 7. *Permittivity of CNT-PU samples measured using impedance analyzer E4991B connected to the DMTF (parallel plate method) in the 10 MHz–1000 MHz frequency range. a: real part; b: imaginary part*

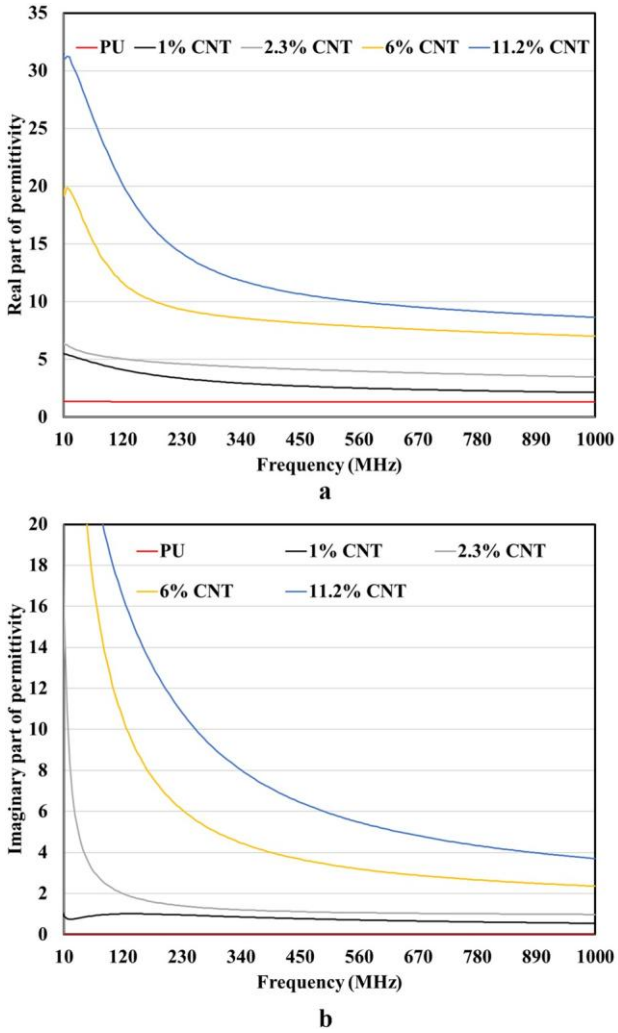

Table 1. *Complex permittivity of CNT-PU samples at 1000 MHz, obtained using the impedance analyzer*

Sample name	Complex permittivity at 1000 MHz	
	Real part	Imaginary part
PU	1.32	0.0059
1 wt.% CNT	2.14	0.55
2.3 wt.% CNT	3.47	0.98
6 wt.% CNT	7.01	2.36
11.2 wt.% CNT	8.65	3.70

The imaginary part of permittivity also increased with increasing CNT content, in agreement with the increment in the AC conductivity as presented in Fig. 6. This observation follows the study by Huang [49]. EM waves convert into electric currents that are resisted by the absorber, generating joule heat that dissipates the EM wave energy [50]. In our study, the presence of the interconnected

Published in : Journal of Materials Science: Materials in Electronics (2025), vol. 36, n°28, 1836
DOI: 10.1007/s10854-025-15900-x
Status : Postprint (Author's version)

network of CNT fillers was confirmed in Sect. 4.1. Hence, increasing the CNT content increased the dissipation of EM wave energy due to the increment in conductivity.

4.4. DIELECTRIC PROPERTIES IN THE 10GHZ–25GHZ FREQUENCY RANGE

The real and imaginary parts of permittivity for the CNT-PU samples in the 10–25 GHz frequency range are shown in Fig. 8. The ε' and ε'' of 6 wt.% and 11.2 wt.% CNT samples continued to decrease with increasing frequency, which can also be attributed to the denser (additional) conductive networks of CNT as described in Sect. 4.1. It is important to note that the cause for the permittivity decrement with frequency in Fig. 7 (MHz range) and Fig. 8 (GHz range) may not have the same origin. The increment of permittivity with CNT concentrations could be explained by the increment of conductivity since CNT is symmetric and does not have dipole moments [51]. Therefore, the impact of dipole polarization in the CNT structure could be neglected, despite that some local dipoles could arise from curvature or defects.

Fig. 8. *Permittivity of CNT-PU samples measured using OECP connected to VNA (obtained using VNA connected to the OECP) in the 10–25 GHz frequency range. a: real part; b: imaginary part*

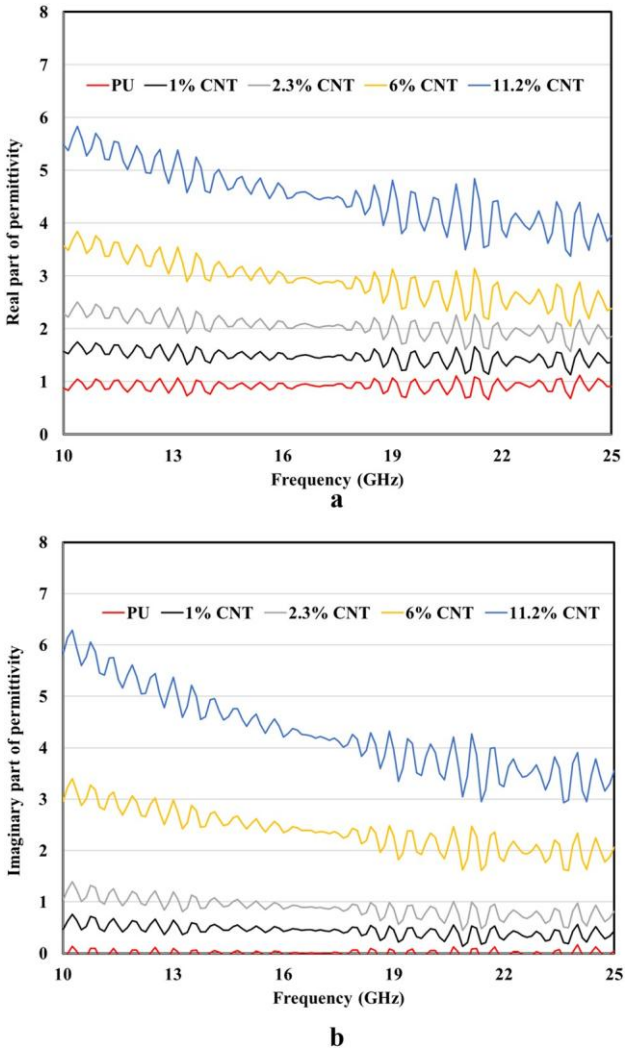

Published in : Journal of Materials Science: Materials in Electronics (2025), vol. 36, n°28, 1836
DOI: 10.1007/s10854-025-15900-x
Status : Postprint (Author's version)

At 25 GHz, the ε' values were 1.37, 1.86, 2.39, and 3.76 for the 1 wt.%, 2.3 wt.%, 6 wt.%, and 11.2 wt.% CNT samples while the corresponding values of ε'' were 0.44, 0.82, 2.07, and 3.56, respectively. This indicates that the ε' and ε'' increased by 36% and 86% with increasing the CNT concentration from 1 wt.% to 2.3 wt.%, respectively.

The relaxation time (τ) decreases as frequency increases; therefore, only certain polarization mechanisms with very low τ can contribute to the permittivity such as hopping and tunnelling. The electrons can tunnel from one CNT to another even when the separations between CNTs are in the order of a few nanometers [52]. The hopping and tunnelling rates could become slow to follow the quickly changing electric field, leading to a reduction in permittivity with frequency above 10 GHz, especially in 11.2 wt.% CNT sample where the rates are very high. Furthermore, the decrement of permittivity with frequency in the 1 wt.% CNT and 2.3 wt.% CNT samples is minor because the hopping and tunnelling rates were initially low. The permittivity of PU continued its stable behaviour over the whole frequency range due to the absence of conductive charges.

4.5. ELECTROMAGNETIC SHIELDING EFFECTIVENESS AND ELECTRIC FIELD DISTRIBUTION

The S_{11} (reflection coefficient) represents the power reflected to port 1, while the S_{21} (transmission coefficient) represents the power transferred from port 1 to port 2 [53]. S_{11} and S_{21} describe the interaction between EM waves and MUT. The scattering parameters (S_{11} and S_{21}) obtained using COMSOL software were used to calculate the return loss (RL), absorption loss (SE_A), reflection loss (SE_R), and total shielding effectiveness (SE_T) using the following equations:

$$RL = 10\log(S_{11}^2) \tag{2}$$

$$SE_A = -10\log\left((S_{11}^2) \div (1 - S_{11}^2)\right) \tag{3}$$

$$SE_R = -10\log(1 - S_{11}^2) \tag{4}$$

$$SE_T = SE_A + SE_R + SE_{MR} \tag{5}$$

Where the SEMR represents the multiple internal reflections, which can be neglected when the total shielding effectiveness is higher than 10 dB [54].

Increasing the CNT content increased the electrical conductivity of the sample, resulting in higher EM reflection and consequently lower return loss, as shown in Fig. 9. This finding is in agreement with the AC conductivity results presented in Fig. 6. The relationship between conductivity and the wave impedance can explain the increment in EM reflection (reduction in RL). The wave impedance (Z) equation is expressed as follows:

$$z = \left((j\omega\mu) \div (\sigma_{ac} + j\omega\varepsilon)\right)^{0.5} \tag{6}$$

Published in : Journal of Materials Science: Materials in Electronics (2025), vol. 36, n°28, 1836
DOI: 10.1007/s10854-025-15900-x
Status : Postprint (Author's version)

Fig. 9. *Return loss of CNT-PU samples in the 18–26.5 GHz frequency range obtained using Eq. 2*

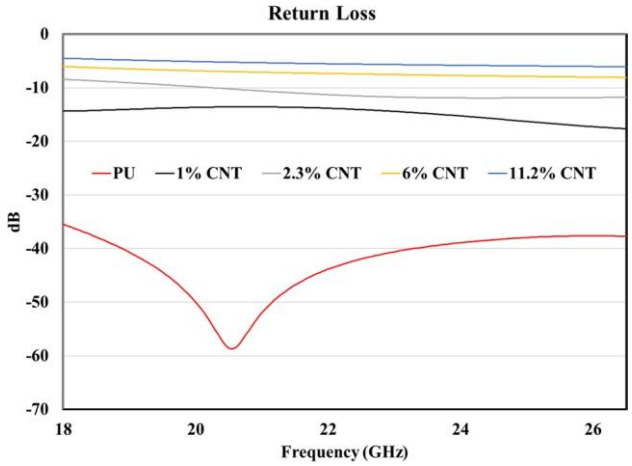

Where $\omega = 2\pi f$ represents the angular frequency of the wave, μ is the magnetic permeability, σ_{ac} is the electrical conductivity of the MUT, and ε is the (real) electric permittivity. The conductivity's increment caused a decrease in the wave impedance with respect to that of air, which in turn increased the EM reflection. Hence, more EM energy is reflected with higher CNT concentration because of the impedance mismatch. The RL values of PU, 1 wt.% CNT, 2.3 wt.% CNT, 6 wt.% CNT, and 11.2 wt.% CNT samples were − 37.7 dB, − 17.63 dB, − 11.80 dB, − 8.08 dB, and − 6.07 dB, respectively. The PU sample had the lowest RL over the whole frequency range because of the good impedance matching between the free space and the PU sample (which has a low value of dielectric constant). On the contrary, increasing the CNT content resulted in higher values of dielectric constant, leading to higher impedance mismatching and consequently higher RL values.

At 26.5 GHz, the SE_T of PU, 1 wt.% CNT, 2.3 wt.% CNT, 6 wt.% CNT, and 11.2 wt.% CNT samples were 0.57 dB, 8.33 dB, 14.20 dB, 30.90 dB, and 42.84 dB, respectively. This means that increasing the CNT content from 0 wt.% CNT (PU) to 1% CNT enhanced the SE_T by around 1361% while the increment from 6 wt.% CNT to 11.2 wt.% only enhanced the SE_T by around 39%. The reason for this drop from 1361 to 39% could be because of the conductive network of CNT which was built on the 1 wt.% CNT sample, as confirmed in Sub Sect. 4.2. Then, increasing the CNT content to the pre-built conductive network can slowly enhance the SE_T.

Published in : Journal of Materials Science: Materials in Electronics (2025), vol. 36, n°28, 1836
DOI: 10.1007/s10854-025-15900-x
Status : Postprint (Author's version)

Fig. 10. *Total shielding effectiveness of CNT-PU samples in the 18–26.5 GHz frequency range, obtained using Eq. 5*

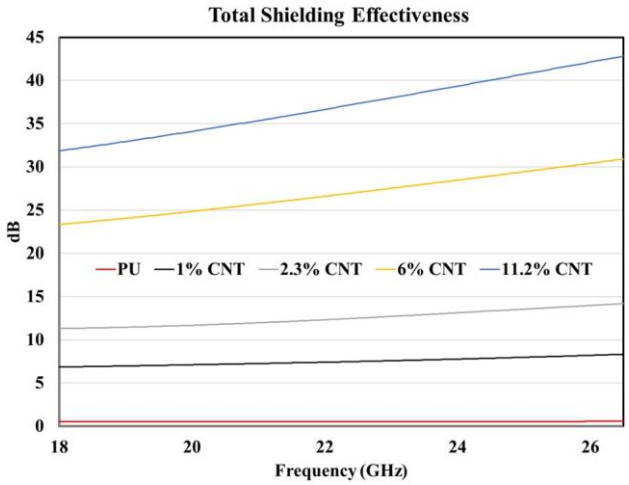

The SE_T of CNT-PU samples increased with increasing frequency and CNT content as shown in Fig. 10. The SE_T increment with increased CNT content can be attributed to the increase in AC conductivity which caused higher energy absorption. Additionally, increasing frequency causes higher ohmic loss per volume unit because the power (current) density normally increases with increasing frequency. Samples with higher CNT concentrations tend to block more EM waves due to the increment in absorption as explained in Sub Sect. 4.3. It is also worth noting that increasing the content of CNT caused an increase in the ascending trend of SE_T values. The SE_T values of PU are almost constant compared to the ones of the 11.2 wt.% CNT sample that ascends steeply. This trend is attributed to the fact that EM waves tend to dissipate more when interacting with absorbing material at higher frequencies.

The good EMI shielding material causes a maximum attenuation of the EM wave by absorption or reflection with inappreciable transmission. When the SE_T of a certain material is 20 dB, this means that there is an attenuation of 99% of the total energy of the incident wave [55]. The EMI shielding requirements depend on the application. For example, the EMI shielding of 15–20 dB is considered an adequate level of shielding for desktop computers and laptops [56]. Our 6 wt.% CNT and 11.2 wt.% CNT samples meet and exceed the required value (20 dB) for the mentioned applications over the whole frequency range. Additionally, the shielding performance of CNT-PU samples can be enhanced by increasing the sample's thickness and/or CNT content.

The contribution of reflection loss to the SE_T is not significant compared to the absorption loss which greatly influenced the SE_T of CNT-PU sample, as presented in Fig. 11. The SE_A contribution to the SE_T of CNT-PU samples was greater at higher frequencies. For example, the SE_A of 1 wt.% CNT sample caused around 97.6% of the SE_T at 18 GHz compared to 99.1% at 26.5 GHz. Such behaviour could be attributed to higher ohmic loss at higher frequencies, leading to higher absorption performance. Hence, our samples are highly preferred in industry because they reduce primary and secondary reflections that can cause unwanted EMI in nearby devices, eliminating the EMI and preventing it from spreading to the environment.

Published in : Journal of Materials Science: Materials in Electronics (2025), vol. 36, n°28, 1836
DOI: 10.1007/s10854-025-15900-x
Status : Postprint (Author's version)

The SE_T results obtained in this study were compared with previously published literature, as presented in Table 2. The SE_T results of our CNT-PU samples surpassed reported results, showing better EM shielding performance.

The CNT concentrations had a significant impact on the electric field (EF) distribution as presented in Fig. 12. The Y axis ranges from − 40 mm to 30 mm. The MUT represents the region from − 10 mm to 0 mm. There was a big change in the EF behaviour in region 3 compared to region 1 for the CNT samples. However, the PU sample did not have a strong impact on the EF, which only countered a slight decrease in intensity. This pattern can be explained by the weak interaction between the electric field and pure PU sample. The permittivity values of PU sample, presented in Figs. 7 and 8, are close to one of free space, leading to a negligible dielectric loss. Therefore, the EF can pass through the PU sample with a very weak attenuation. On the other hand, the intensity of the EF in region 3 decreased with increasing the CNT content which enhanced the AC conductivity and caused more interaction with the EF. The permittivity results shown in Figs. 7 and 8 are consistent with the EF distribution shown in Fig. 12. Samples with higher permittivity attenuated the EM signal more effectively, leading to a lower EF in region 3 as the CNT content increased. The EF could not enter the 11.2 wt.% sample because it had the highest concentration of CNT, which causes more reflection and losses. The regions of strong electric are totally separated in the 11.2 wt.% CNT samples compared to the 1 wt.% CNT sample where the regions of strong EF are connected to each other with lower values (around 5×10^3 V/m). Increasing the content of CNT caused more concentrations of the electric field at specific regions.

Published in : Journal of Materials Science: Materials in Electronics (2025), vol. 36, n°28, 1836
DOI: 10.1007/s10854-025-15900-x
Status : Postprint (Author's version)

Fig. 11. *The contribution of SER and SEA to the SET of CNT-PU samples at certain frequencies of 18 GHz, 20 GHz, 22 GHz, 24 GHz , and 26.5 GHz, calculated using Eqs. 3–5*

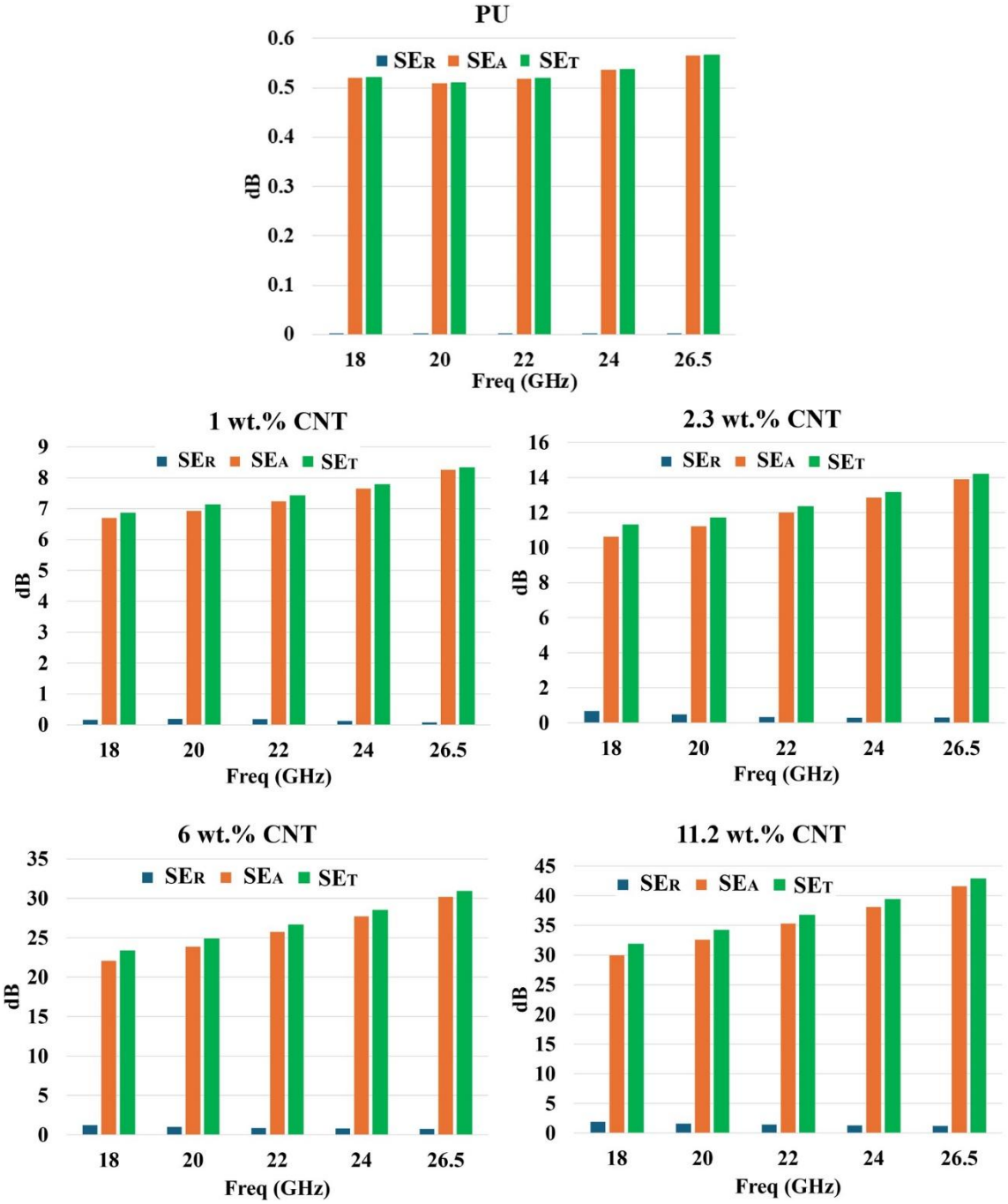

The EF distribution analysis can help in designing EM shielding materials such as electronic packaging, electrical enclosures, and gaskets. Such simulations are important before producing the prototype to predict the failures that could lead to an extensive EF in some regions. The EMI shielding material is usually classified as low quality if the EF intensity is slightly decreased after passing through it, compared to a high-quality shielding material, which strongly decreases the EF intensity.

Published in : Journal of Materials Science: Materials in Electronics (2025), vol. 36, n°28, 1836
DOI: 10.1007/s10854-025-15900-x
Status : Postprint (Author's version)

These simulations can enhance the design accuracy and reduce the fabrication cost, leading to optimal EMI shielding materials.

Table 2. *The comparison of SET results with previous studies*

Materials and filler percentage	Thickness (mm)	SE_T (dB)	Frequency (GHz)	Ref
CNT/PU with 4.35% of CNT without buckling structures (UCNPF) (foamed)	10	≈ 25	12	[57]
CNT-PU with 25% of CNT (foamed)	2	≈ 30	12	[58]
CNT-PU with 9% of CNT (foamed)	3.4	≈ 9	12	[59]
Polycarbonate—carbon nanotubes (PC-CNT) with 1% of CNT (unfoamed)	5	≈ 8	18	[60]
polycarbonate—poly(styrene-*co*-acrylonitrile) (PC-SAN) with 3% of CNT (unfoamed)	2	≈ 20	18	[61]
Polyethylene/Poly(vinylidene fluoride)/Fe_3O_4/Carbon nanotubes (PE/PVDF/Fe_3O_4/CNTs) with 10% CNT (foamed)	2.6	≈ 29	26.5	[62]
CNT-PU with 6% CNT	10	30.9	26.5	This work
CNT-PU with 11.2% CNT	10	42.8	26.5	This work

5. Conclusion

CNT-PU foam nanocomposites with different CNT contents were successfully prepared and characterized for absorption-based EM shielding applications. The measurements were conducted over a broad range of frequencies to cover a wide range of applications. The impact of increasing the CNT content on the AC conductivity and permittivity was investigated using different measurement techniques. Additionally, the effects of CNT content on the scattering parameters (S_{11}, S_{21}) and the intensity of electric field distribution of CNT-PU samples were also investigated using COMSOL Multiphysics. This study employed the Dielectric Material Test Fixture, for the first time, to measure the permittivity of foam samples thanks to our 3D-printed holder. The SEM images confirmed that the CNTs established interconnected and evenly distributed networks on the PU surface of all CNT-PU samples. The AC conductivity increased with increasing frequency and CNT content, and the highest value of 0.0068 S/cm was recorded for 11.2 wt.% CNT sample at 10 MHz. Additionally, the permittivity (real and imaginary parts) of our samples increased with increasing CNT content but decreased with increasing frequency. At 1000 MHz, the complex permittivity increased from 1.32—j 0.0059 for PU foam to 8.65—j 3.70 for 11.2 wt.% CNT sample. Similarly, the same sample recorded the highest complex permittivity value of 3.76—j 3.56 at 25 GHz. The total shielding effectiveness was significantly improved by the conductive networks, confirmed by SEM images, located on the PU surfaces. Two of our prepared samples (6 wt.% CNT and 11.2 wt.% CNT) fulfilled the standard

Published in : Journal of Materials Science: Materials in Electronics (2025), vol. 36, n°28, 1836
DOI: 10.1007/s10854-025-15900-x
Status : Postprint (Author's version)

commercial requirements for EMI shielding applications in the 18–26.5 GHz frequency range. The total shielding effectiveness was also greatly enhanced with the increment of CNT amount. The intensity of the electric field passing through the samples significantly dropped with increasing the CNT filler concentration. The prepared samples exhibited a strong absorption performance in dissipating EM energy; such a feature is very advantageous and preferred in the EMI shielding industry because it reduces the EMI in the environment. This study could be performed using different foam matrices with higher values of permittivity. Different conductive fillers could also be used to enhance the dielectric properties of shielding materials.

Fig. 12. *Electric field distribution obtained using COMSOL Multiphysics at 26.5 GHz. a: PU sample, b: 1 wt.% CNT, c: 2.3 wt.% CNT, d: 6 wt.% CNT, and e: 11.2 wt.% CNT*

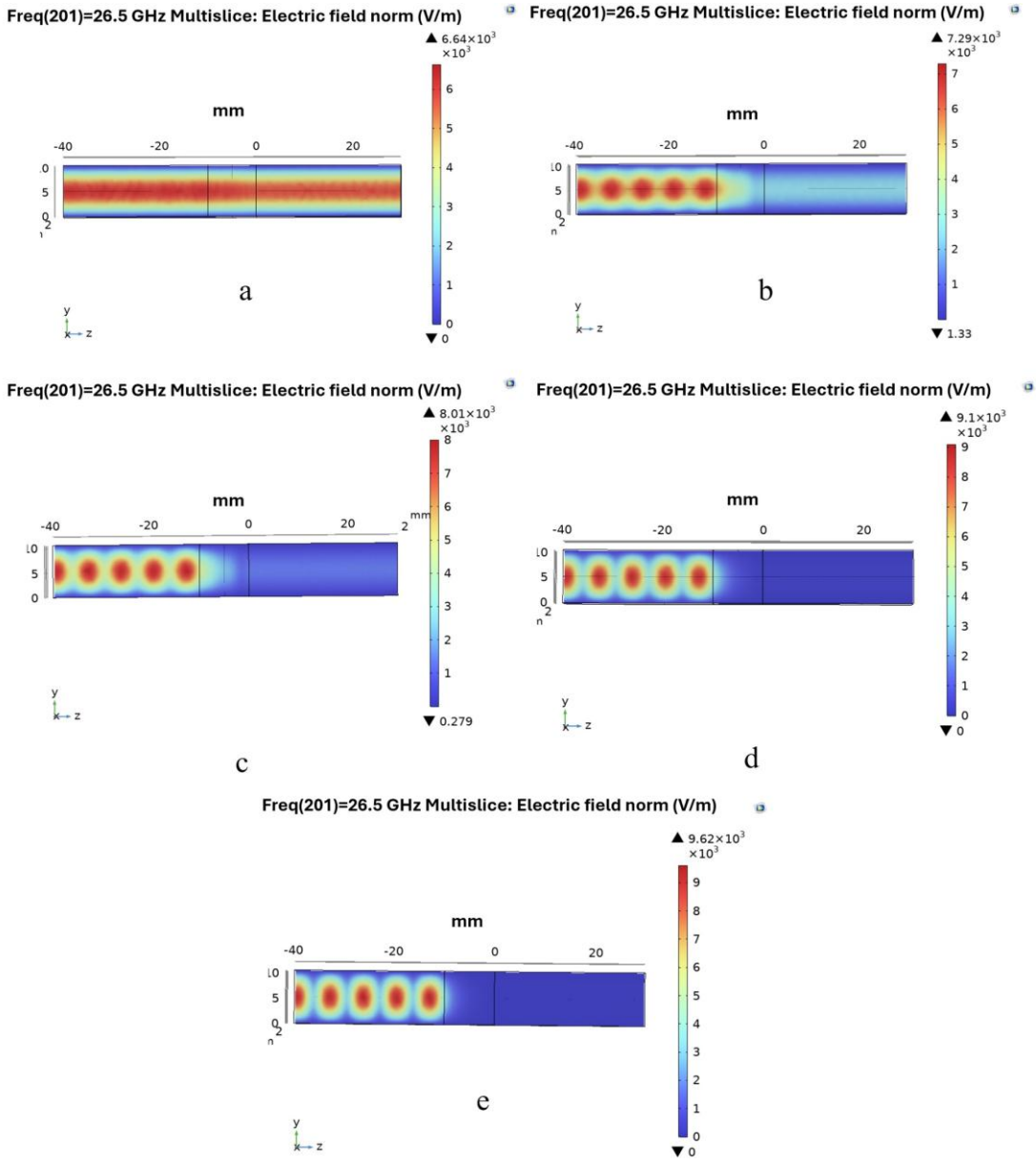

Published in : Journal of Materials Science: Materials in Electronics (2025), vol. 36, n°28, 1836
DOI: 10.1007/s10854-025-15900-x
Status : Postprint (Author's version)

ACKNOWLEDGEMENTS

The authors thank Pascal Simon and Benoît Hubert from the Welcome technological platform of UCLouvain for their great support in the measurements of CNT-PU samples. Benoît Hubert designed and fabricated the 3D-printed holder for the DMTF. The authors also thank Delphine Magnin from IMCN of UCLouvain for conducting SEM characterization. The works of I. Huynen and C. Detrembleur as research directors are funded by the National Fund for Scientific Research (FNRS, Belgium).

AUTHOR CONTRIBUTIONS

Ahmad Khamis: Writing—review & editing, Writing—original draft, Data curation, Investigation, Formal analysis. Laetitia Urbanczyk: Conceptualization, Methodology, Investigation, Writing—review & editing. Christophe Detrembleur: Project administration, Methodology, Resources, Writing—review & editing, Supervision, Funding acquisition. Isabelle Huynen: Writing—review & editing, Writing—original draft, Formal analysis, Project administration; Resources, Supervision, Funding acquisition. All authors approved the final version of this article.

FUNDING

This work was performed in the frame of the UP_Plastics project co-funded by the European Union and the Walloon Region as part of the FEDER 2021–2027 Program.

DATA AVAILABILITY

The data that support the findings of this study are available upon reasonable request.

DECLARATIONS

Competing interests The authors have no relevant financial or non-financial interests to disclose.

Published in : Journal of Materials Science: Materials in Electronics (2025), vol. 36, n°28, 1836
DOI: 10.1007/s10854-025-15900-x
Status : Postprint (Author's version)

References

[1] S. Meena, N. Kumari, V. Gahlaut, C. Shekhar, S. Mitra, and U. K. Dwivedi, Electrical and EMI shielding studies of ferrite/MWCNTs/PVDF composite. *J. Appl. Poly. Sci.* pp. e56446.

[2] H. Kim, S. Jeon, Y.S. Cho, C. Huang, S. Na, J. Lee, Y. Chung, J. Kang, S.W. Kim, D. Choi, Polydopamine-coated iron-nickel alloy and epoxy composites for electromagnetic interference shielding. J. Appl. Polym. Sci. **141**(44), e56187 (2024)

[3] M. Magioli, B. Soares, A. Sirqueira, M. Rahaman, D. Khastgir, EMI shielding effectiveness and dielectrical properties of SBS/PAni. DBSA blends: effect of blend preparation. J. Appl. Polym. Sci. **125**(2), 1476–1485 (2012)

[4] R. Hsissou, R. Seghiri, Z. Benzekri, M. Hilali, M. Rafik, A. Elharfi, Polymer composite materials: a comprehensive review. Compos. Struct. **262**, 113640 (2021)

[5] R. K. Mishra, M. G. Thomas, J. Abraham, K. Joseph, and S. Thomas, 2018 Electromagnetic interference shielding materials for aerospace application: a state of the art. *Adv. Mater. Electromag. Shield. Fundament. Prop. Appl.* pp. 327–365.

[6] M.H. Al-Saleh, U. Sundararaj, Electromagnetic interference shielding mechanisms of CNT/polymer composites. Carbon **47**(7), 1738–1746 (2009)

[7] M.G. Jang, S.C. Ryu, K.J. Juhn, S.K. Kim, W.N. Kim, Effects of carbon fiber modification with multiwall CNT on the electrical conductivity and EMI shielding effectiveness of polycarbonate/carbon fiber/CNT composites. J. Appl. Polym. Sci. **136**(14), 47302 (2019)

[8] L. Guohua, Z. Zhiyong, and W. Yangang, 2025 Research progress on highly conductive polymer composites based on carbon-based nanofillers. *Poly. Comp*.

[9] S. Bayda, M. Adeel, T. Tuccinardi, M. Cordani, F. Rizzolio, The history of nanoscience and nanotechnology: from chemical–physical applications to nanomedicine. Molecules **25**(1), 112 (2019)

[10] X. Cheng, 2014 Nanostructures: fabrication and applications. *Nanolithography*. pp. 348–375: Elsevier.

[11] S. Malik, K. Muhammad, Y. Waheed, Nanotechnology: a revolution in modern industry. Molecules **28**(2), 661 (2023)

[12] S. Alfei, G. Zuccari, Last fifteen years of nanotechnology application with our contribute. Nanomaterials **15**(4), 265 (2025)

[13] S.A. Zaidi, J.H. Shin, Recent developments in nanostructure based electrochemical glucose sensors. Talanta **149**, 30–42 (2016)

[14] N. Chikyu, T. Nakano, G. Kletetschka, Y. Inoue, Excellent electromagnetic interference shielding characteristics of a unidirectionally oriented thin multiwalled carbon nanotube/ polyethylene film. Mater. Des. **195**, 108918 (2020)

[15] V. S. Eswaraiah, Venkataraman; Ramaprabhu, Sundara, 2011 Functionalized graphene–PVDF foam composites for EMI shielding. *Macromol. Mater. Eng.* 296(10): 894–898

Published in : Journal of Materials Science: Materials in Electronics (2025), vol. 36, n°28, 1836
DOI: 10.1007/s10854-025-15900-x
Status : Postprint (Author's version)

[16] S. Chen, K. Li, G. Wang, W. Ding, X. Zhang, Y. Zhao, Y. Yang, J. Chen, Microcellular foamed bilayer iPP/CNTs-HDPE/CNTs nanocomposites for electromagnetic interference shielding application. J. Polym. Res. **31**(12), 357 (2024)

[17] S. Sultana, M. Rahaman, and M. R. Chandan, 2025 "Enhancing EMI Shielding Efficiency of Polyurethane Foam by Incorporating MWCNT-Decorated Hollow Glass Microspheres," *ACS omega*.

[18] C.K. Kum, Y.-T. Sung, M.S. Han, W.N. Kim, H.S. Lee, S.-J. Lee, J. Joo, Effects of morphology on the electrical and mechanical properties of the polycarbonate/multiwalled carbon nanotube composites. Macromol. Res. **14**, 456–460 (2006)

[19] J.-M. Thomassin, C. Pagnoulle, L. Bednarz, I. Huynen, R. Jerome, C. Detrembleur, Foams of polycaprolactone/MWNT nanocomposites for efficient EMI reduction. J. Mater. Chem. **18**(7), 792–796 (2008)

[20] K. Chizari, M. Arjmand, Z. Liu, U. Sundararaj, D. Therriault, Three-dimensional printing of highly conductive polymer nanocomposites for EMI shielding applications. Mater. Today Commun. **11**, 112–118 (2017)

[21] S. Sultana, M.R. Chandan, Enhanced EMI shielding efficiency of graphene nanoplatelets and glass sphere composite-loaded ultralight weight flexible polyurethane foam. Polym. Adv. Technol. **35**(10), e6611 (2024)

[22] S. Jafarzadeh, A. Farzaneh, V. Haddadi-Asl, I.S. Jouibari, A review on electrically conductive polyurethane nanocomposites: from principle to application. Polym. Compos. **44**(12), 8266–8302 (2023)

[23] Z.E. Zadeh, A. Solouk, M. Shafieian, M.H. Nazarpak, Electrospun polyurethane/carbon nanotube composites with different amounts of carbon nanotubes and almost the same fiber diameter for biomedical applications. Mater. Sci. Eng. C **118**, 111403 (2021)

[24] K. Nakagawa, 2011 "Foam materials made from carbon nanotubes," *Carbon Nanotubes-From Research to Applications*.

[25] Q. Xu, W. Zhang, Improvement of the electromechanical properties of thermoplastic polyurethane composite by ionic liquid modified multiwall carbon nanotubes. E-Polymers **21**(1), 166–178 (2021)

[26] D. Zhang, H. Yang, J. Pan, B. Lewis, W. Zhou, K. Cai, A. Benatar, L.J. Lee, J.M. Castro, Multi-functional CNT nanopaper polyurethane nanocomposite fabricated by ultrasonic infiltration and dip soaking processes. Compos. B Eng. **182**, 107646 (2020)

[27] X. Huang, D. Yu, S. Wang, Microwave absorption properties of multi-walled carbon nanotubes/carbonyl iron particles/polyurethane foams. Materials **15**(16), 5690 (2022)

[28] E. Zawadzak, M. Bil, J. Ryszkowska, S.N. Nazhat, J. Cho, O. Bretcanu, J.A. Roether, A.R. Boccaccini, Polyurethane foams electrophoretically coated with carbon nanotubes for tissue engineering scaffolds. Biomed. Mater. **4**(1), 015008 (2008)

[29] X. Wang, H. Li, T. Wang, X. Niu, Y. Wang, S. Xu, Y. Jiang, L. Chen, H. Liu, Flexible and high-performance piezoresistive strain sensors based on multi-walled carbon nanotubes@ polyurethane foam. RSC Adv. **12**(22), 14190–14196 (2022)

[30] X.-C. Zhang, F. Scarpa, R. McHale, A.P. Limmack, H.-X. Peng, Carbon nano-ink coated open cell polyurethane foam with micro-architectured multilayer skeleton for damping applications. RSC Adv. **6**(83), 80334–80341 (2016)

[31] Tewari, S. Gandla, S. Bohm, C.R. McNeill, D. Gupta, Highly exfoliated MWNT–rGO ink-wrapped polyurethane foam for piezoresistive pressure sensor applications. ACS Appl. Mater. Interf. **10**(6), 5185–5195 (2018)

[32] M. Nabeel, M. Mousa, B. Viskolcz, B. Fiser, L. Vanyorek, Recent advances in flexible foam pressure sensors: manufacturing, characterization, and applications–a review. Polym. Rev. **64**(2), 449–489 (2024)

[33] H. Xu, Y. Zhang, and F. Zheng, 2009 "Study on measuring method of dielectric spectroscopy for polymer dielectrics," in 2009 IEEE 9th International Conference on the Properties and Applications of Dielectric Materials. pp. 922–925.

[34] Hosseinbeig, S. Marathe, D. Pommerenke, Characterization of relative complex permittivity and permeability for magneto-dielectric sheets. IEEE Trans. Electromagn. Compat. **60**(6), 1786–1794 (2017)

[35] S. Hang, and W. Xue-tao, "Application of COMSOL multiphysics in thermal effect analysis of electromagnetic active vibration absorber," in IOP Conference Series: Materials Science and Engineering, 2017, pp. 012037.

[36] Akdagli, K. Guney, New wide-aperture-dimension formula obtained by using a particle swarm optimization for optimum gain pyramidal horns. Microw. Opt. Technol. Lett. **48**(6), 1201–1205 (2006)

[37] H.-Z. Ma, J.-N. Zhao, R. Tang, Y. Shao, K. Ke, K. Zhang, B. Yin, M.-B. Yang, Polypyrrole@ CNT@ PU conductive sponge-based triboelectric nanogenerators for human motion monitoring and self-powered ammonia sensing. ACS Appl. Mater. Interf. **15**(47), 54986–54995 (2023)

[38] D. Wu, M. Wei, R. Li, T. Xiao, S. Gong, Z. Xiao, Z. Zhu, Z. Li, A percolation network model to predict the electrical property of flexible CNT/PDMS composite films fabricated by spin coating technique. Compos. B Eng. **174**, 107034 (2019)

[39] P.R. Connolly, M. Josh, K.T. O'Neill, S.J. Seltzer, M.O. Wigand, M.B. Clennell, E.F. May, M.L. Johns, Dielectric polarization studies in partially saturated shale cores. J. Geophys. Res. Solid Earth **124**(11), 10721–10734 (2019)

[40] A.S. Hoang, Electrical conductivity and electromagnetic interference shielding characteristics of multiwalled carbon nanotube filled polyurethane composite films. Adv. Nat. Sci. Nanosci. Nanotechnol. **2**(2), 025007 (2011)

[41] I.V. Novikov, D.V. Krasnikov, A.M. Vorobei, Y.I. Zuev, H.A. Butt, F.S. Fedorov, S.A. Gusev, A.A. Safonov, E.V. Shulga, S.D. Konev, Multifunctional elastic nanocomposites with extremely low concentrations of single-walled carbon nanotubes. ACS Appl. Mater. Interf. **14**(16), 18866–18876 (2022)

[42] M. Yanılmaz, A.S. Sarac, A review: effect of conductive polymers on the conductivities of electrospun mats. Text. Res. J. **84**(12), 1325–1342 (2014)

[43] S. Bronnikov, S. Kostromin, M. Asandulesa, D. Pankin, A. Podshivalov, Interfacial interactions and interfacial polarization in polyazomethine/MWCNTs nanocomposites. Compos. Sci. Technol. **190**, 108049 (2020)

[44] T. Durance, and P. Yaghmaee, 2011 "4.51-microwave dehydration of food and food ingredients," *Comprehensive biotechnology*, pp. 617–628.

[45] J. Wu, Y. Gao, W. Hu, Z. Lu, Influence of carbon nanotubes on the absorption performance and mechanical behavior of basalt fiber composite materials. Polym. Compos. **46**(4), 3109–3121 (2025)

[46] B. Wang, Y. Liu, M. Dong, and G. Zuo, "Study on changing the dielectric constant and radar reflection of foamed polyurethane by adding graphite," in Journal of Physics: Conference Series, 2021, pp. 012004.

[47] K. Shehzad, Z.-M. Dang, M.N. Ahmad, R.U.R. Sagar, S. Butt, M.U. Farooq, T.-B. Wang, Effects of carbon nanotubes aspect ratio on the qualitative and quantitative aspects of frequency response of electrical conductivity and dielectric permittivity in the carbon nanotube/polymer composites. Carbon **54**, 105–112 (2013)

[48] M.C. Sekhar, P. Kondaiah, S.J. Chandra, G.M. Rao, S. Uthanna, Effect of substrate bias voltage on the structure, electric and dielectric properties of TiO_2 thin films by DC magnetron sputtering. Appl. Surf. Sci. **258**(5), 1789–1796 (2011)

[49] B. Huang, J. Yue, B. Fan, Y. Liu, X. Huang, Vertical carbon nanotubes arrays with controlled morphology on silicon carbide fibers for electromagnetic wave absorption. Ceram. Int. **48**(13), 19375–19381 (2022)

[50] M. Qin, L. Zhang, H. Wu, Dielectric loss mechanism in electromagnetic wave absorbing materials. Adv. Sci. **9**(10), 2105553 (2022)

[51] S. P. Walch, "The bonding of NOz, NH, and CHI" to models of a (10, O) carbon nanotube."

[52] A. Mora, P. Verma, S. Kumar, Electrical conductivity of CNT/polymer composites: 3D printing, measurements and modeling. Compos. B Eng. **183**, 107600 (2020)

[53] F. Caspers, 2012 "RF engineering basic concepts: S-parameters," *arXiv preprint* arXiv: 1201. 2346.

[54] Y. Luo, Y. Guo, C. Wei, J. Chen, G. Zhao, Q. Yuan, Y. Zhu, Lightweight, compressible, and stretchable composite foams for ultra-efficient and high-stable electromagnetic interference shielding materials. Carbon **215**, 118480 (2023)

[55] R.R. Mohan, S.J. Varma, J. Sankaran, Impressive electromagnetic shielding effects exhibited by highly ordered, micrometer thick polyaniline films. Appl. Phys. Lett. (2016). https:// doi. org/ 10. 1063/1. 49457 91

[56] M.H. Al-Saleh, G.A. Gelves, U. Sundararaj, Copper nanowire/polystyrene nanocomposites: lower percolation threshold and higher EMI shielding. Compos. A Appl. Sci. Manuf. **42**(1), 92–97 (2011)

[57] K. Huang, M. Chen, G. He, X. Hu, W. He, X. Zhou, Y. Huang, Z. Liu, Stretchable microwave absorbing and electromagnetic interference shielding foam with hierarchical buckling induced by solvent swelling. Carbon **157**, 466–477 (2020)

[58] G. Sang, P. Xu, T. Yan, V. Murugadoss, N. Naik, Y. Ding, Z. Guo, Interface engineered microcellular magnetic conductive polyurethane nanocomposite foams for electromagnetic interference shielding. Nano-Micro Letters **13**(1), 153 (2021)

[59] Z. Lei, D. Tian, X. Liu, J. Wei, K. Rajavel, T. Zhao, Y. Hu, P. Zhu, R. Sun, C.-P. Wong, Electrically conductive gradient structure design of thermoplastic polyurethane composite foams for efficient

Published in : Journal of Materials Science: Materials in Electronics (2025), vol. 36, n°28, 1836
DOI: 10.1007/s10854-025-15900-x
Status : Postprint (Author's version)

electromagnetic interference shielding and ultra-low microwave reflectivity. Chem. Eng. J. **424**, 130365 (2021)

[60] K. Sushmita, A.V. Menon, S. Sharma, A.C. Abhyankar, G. Madras, S. Bose, Mechanistic insight into the nature of dopants in graphene derivatives influencing electromagnetic interference shielding properties in hybrid polymer nanocomposites. J. Phys. Chem. C **123**(4), 2579–2590 (2019)

[61] S.P. Pawar, S. Bose, Extraordinary synergy in attenuating microwave radiation with cobalt-decorated graphene oxide and carbon nanotubes in polycarbonate/poly (styrene-coacrylonitrile) blends. ChemNanoMat **1**(8), 603–614 (2015)

[62] Y. Zhao, J. Hou, Z. Bai, Y. Yang, X. Guo, H. Cheng, Z. Zhao, X. Zhang, J. Chen, C. Shen, Facile preparation of lightweight PE/PVDF/Fe3O4/CNTs nanocomposite foams with high conductivity for efficient electromagnetic interference shielding. Compos. A Appl. Sci. Manuf. **139**, 106095 (2020)